

Supporting Information for:

**Multispectral Thin Film Biosensing and Quantitative Imaging Using 3D Plasmonic Crystals**

Matthew E. Stewart<sup>†ξ</sup>, Jimin Yao<sup>‡ξ</sup>, Joana Maria<sup>‡</sup>, Stephen K. Gray<sup>¶</sup>, John A. Rogers<sup>†‡</sup>,  
and Ralph G. Nuzzo<sup>†‡\*</sup>

<sup>†</sup> Department of Chemistry  
University of Illinois at Urbana-Champaign  
Urbana, Illinois 61801

<sup>‡</sup> Department of Materials Science and Engineering  
University of Illinois at Urbana-Champaign  
Urbana, Illinois 61801

<sup>¶</sup> Chemistry Division and Center for Nanoscale Materials  
Argonne National Laboratory  
Argonne, Illinois 60439

\* Corresponding author

<sup>ξ</sup> These authors contributed equally to this work.

## **Table of Contents**

This Word document contains supporting Figures S1-S6.

Figure S1...page S3

Figure S2...pages S4

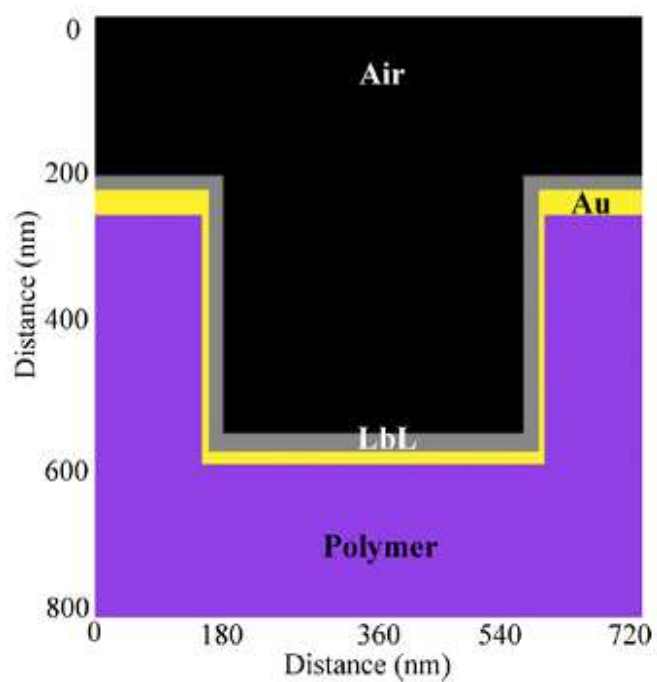
Figure S3...pages S5-S6

Figure S4...page S7

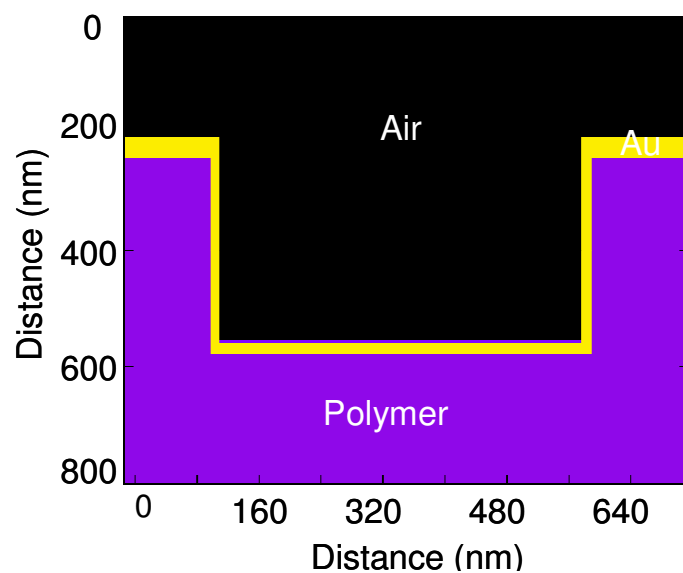
Figure S5 and associated text...pages S8-S10

Figure S6...page S11

References...page S12



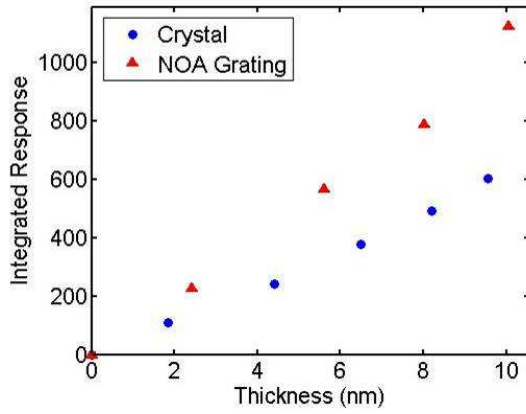
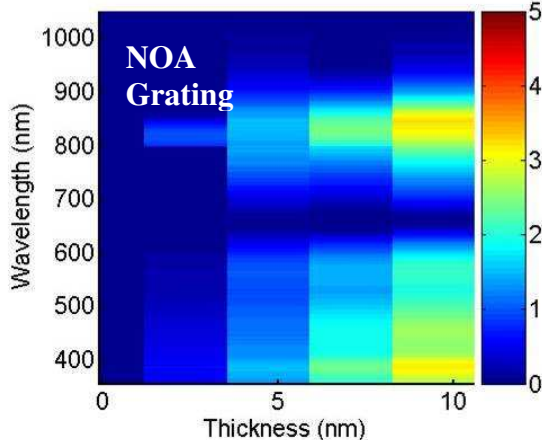
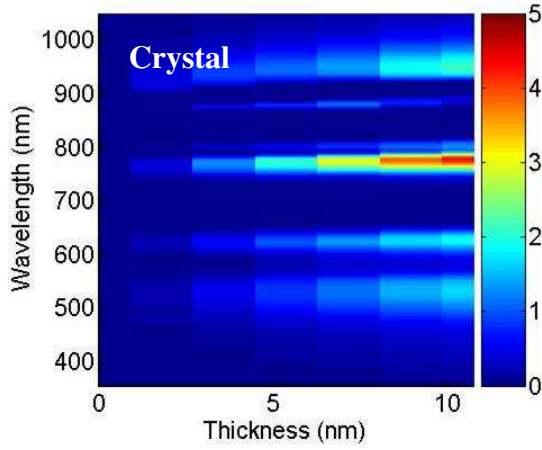
**Figure S1.** Schematic illustration of a cross-sectional cut through the x-z plane of the unit cell used in the FDTD calculations. The grey area labeled LbL corresponds to the alternating PAH and PSS polyelectrolyte layers, which are modeled as a single effective medium.



**Figure S2.** A schematic illustration of a cross-sectional cut through a plasmonic crystal with gold thicknesses on the top of the crystal and sidewalls and bottoms of the nanowells of 35, 12, and 20 nm, respectively.

(a)

$$R_{th}(\lambda) = T_{th}(\lambda) - T_o(\lambda)$$



(b)

$$R_{th}(\lambda) = \frac{T_{th}(\lambda) - T_o(\lambda)}{T_o(\lambda)}$$

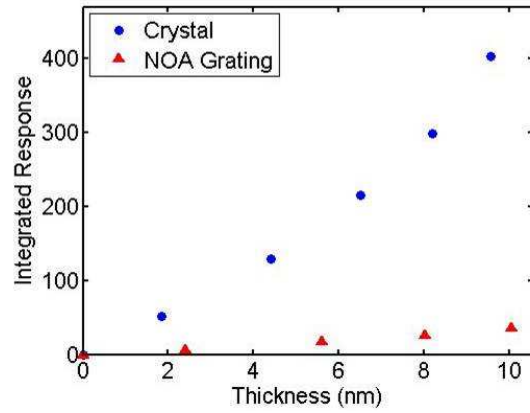
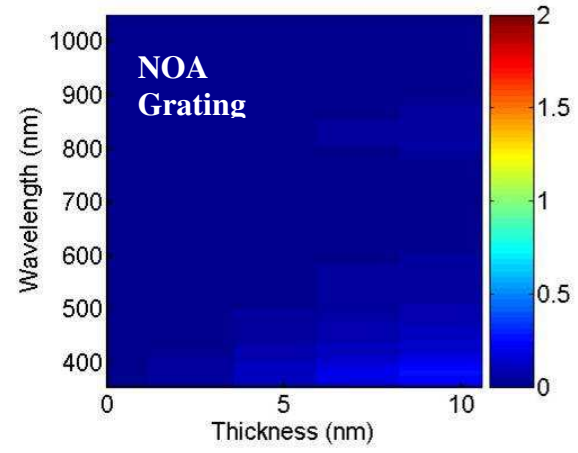
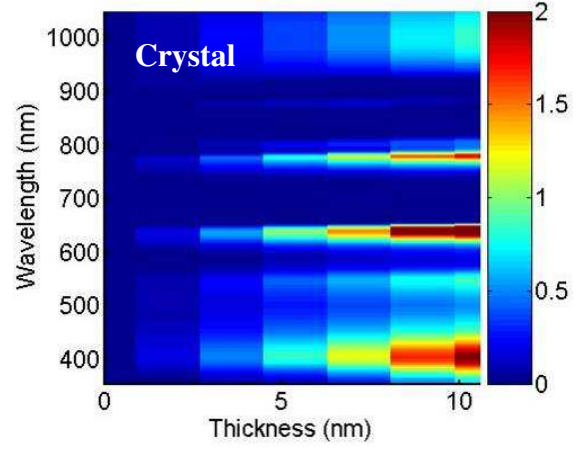


**Figure S3.** Comparison of the optical response of a ~728 nm periodicity plasmonic crystal with (crystal) and without (NOA) a 70 nm gold film to increasing polyelectrolyte film thicknesses measured in air. The **top and middle panels** present difference maps of the gold plasmonic crystal and the NOA grating, respectively. The equations used to calculate the difference maps in columns **(a)** and **(b)** are shown at the top of the columns. In **(a)** the change in transmission due to increasing polyelectrolyte film thickness is not normalized by the initial transmission ( $T_0$ ) of the crystal – an approach to multispectral sensing described by us previously[1], where as in **(b)** the change in transmission is normalized by  $T_0$  to compensate for Fresnel reflections (see Eq. 1 in the main text of this work). The **bottom panels** in (a) and (b) show the corresponding integrated responses of the difference maps in the top and middle panels, where the integrated response is calculated using Eq. 2 in the main text. The sensitivity of the crystal and NOA grating is determined by taking the derivative of the curves in the bottom panels of (a) and (b). The bottom panel of (a) shows that the NOA grating, which does not support plasmonic modes, is more sensitive than the plasmonic crystal to surface binding events when the change in transmission is not normalized by  $T_0$ . The bottom panel of (b), however, shows that the plasmonic crystal is more sensitive than the NOA grating when the change in transmission is normalized by  $T_0$ . This result can be explained on the basis of Fresnel effects, where absolute changes in transmission scale with the initial magnitude of the signal or transmission of the sensor. Figure S4 shows that the transmission of an NOA grating is much greater than the transmission of a plasmonic crystal covered with a 70 nm gold film.

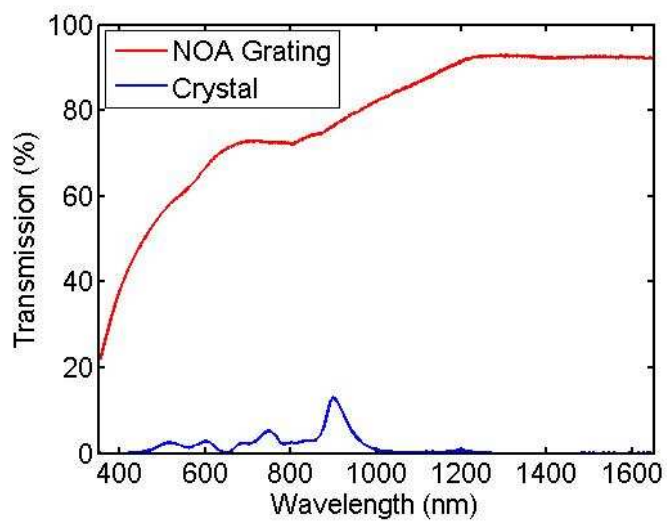


**Figure S4.** Normal incidence transmission spectra of an NOA grating and plasmonic crystal covered with a 70 nm thick gold film.

**Figure S5 and associated text:**

A figure of merit (FOM) commonly used to compare the sensitivity of plasmonic sensors is the bulk refractive index sensitivity, which is determined by measuring changes in the position or intensity of a single resonance peak or wavelength, respectively, as the bulk refractive index of the fluid in contact with the SPR sensor is changed.[2] The 3D plasmonic architectures described in this work yield much more complex optical responses than traditional LSPR and SPR sensors and exhibit multiple spectral features (due to the excitation of LSPRs, BW-SPPs, WAs, and couplings of these features) that all shift in position and intensity as the refractive index of the contacting solution is changed.[1] The commonly used analytical protocol and FOMs that describe the sensitivity of plasmonic sensors at single wavelengths or resonances, therefore do not fully capture the sensitivity of the 3D plasmonic crystals because it ignores the information/signal associated with the multiple features in the spectra. We have developed a type of full, multispectral analysis and associated sensitivity metric that exploits this information to enhance the sensing capabilities of 3D plasmonic crystals as is described below.[1,3]

The multispectral sensitivity of two 3D plasmonic crystals with different gold thicknesses to changes in bulk refractive index is shown in Figure S5(a) and S5(b) below:



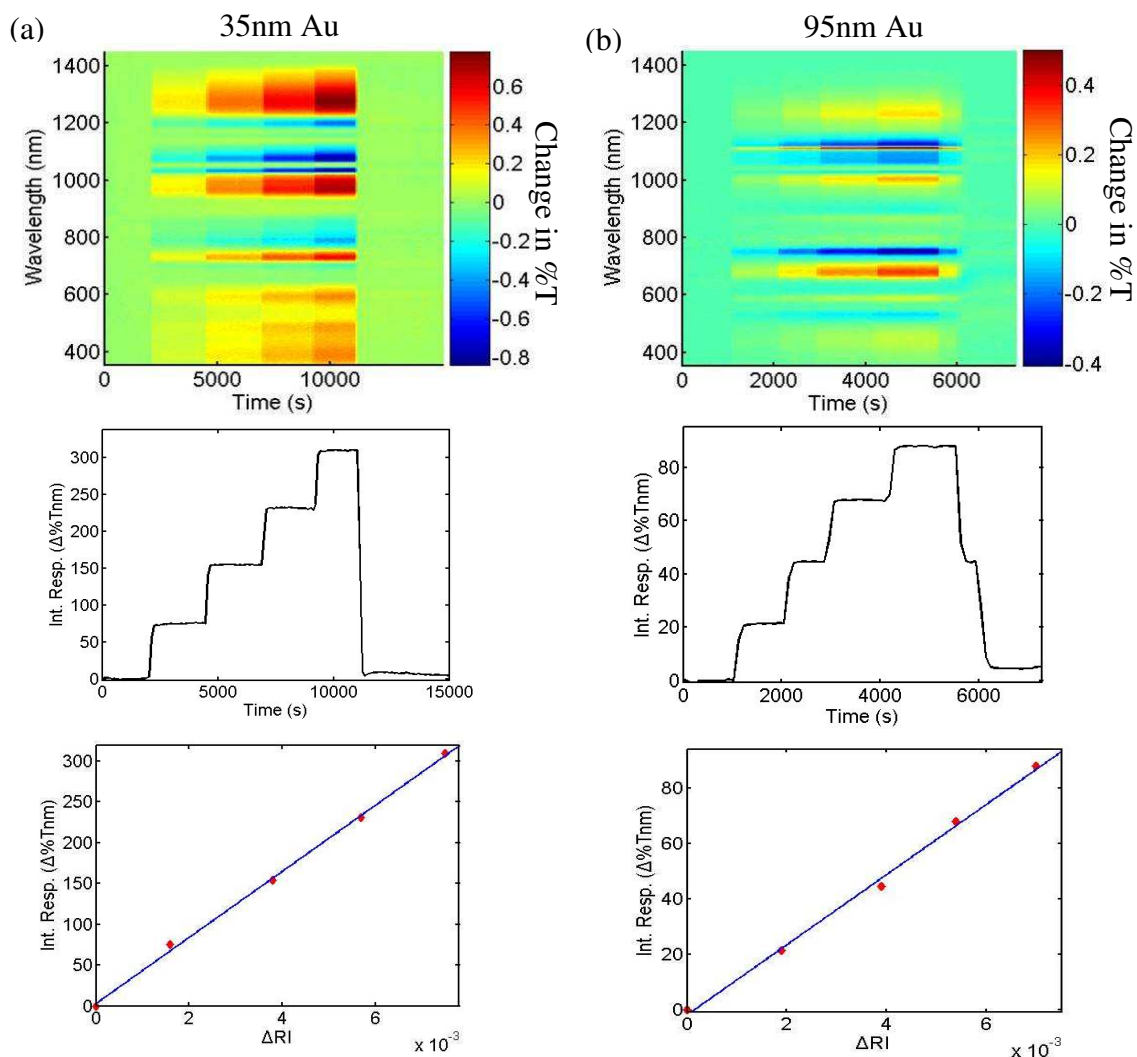


**Figure S5.** Multispectral response of two 3D plasmonic crystals ( $\sim 730$  nm periodicity) with (a) 35 and (b) 95 nm thick gold films to increasing concentrations of polyethylene glycol solutions (PEG). The top panels show color contour plots of the changes in transmission (T) as a function of wavelength and time as solutions of increasing concentration of PEG are injected into the flow cell (the injection sequence is 0, 1.4, 2.8, 4.2, 5.6, and 0% (wt/wt) PEG). The middle panels show the integrated multispectral plasmonic response as a function of time calculated using equation S1. The bottom panel shows the linear correlation between the integrated responses of the crystals to the changes in refractive index. The slope of the lines yield the integrated multispectral bulk refractive index sensitivity, which are  $\sim 41,000$  and  $\sim 13,000$  (%T)nm/RIU for the 35 and 95nm thick gold crystals, respectively.

Spectra were collected as a function of time as solutions of increasing concentration – and thus refractive index – of poly(ethylene glycol) (PEG, MW=10,000g/mol) were passed through a fluid-flow cell containing the 3D crystals. The series of spectra were then referenced to the initial spectrum at time  $t=0$  to generate the difference maps in the top panels of Figure S5, which show the changes in transmission (due to changes in peak position and intensity) over a broad range of wavelengths as the refractive index of the solution in the flow cell was increased. Measuring the change in intensity at one wavelength or the change in position of one peak in the spectral response of the crystals – the common analytical protocol for SPR sensors that exhibit single resonances – to refractive index changes ignores the information associated with the other peaks in the spectra. A more appropriate FOM for these 3D crystals is one that accounts for both the wavelength and intensity-based contributions to the optical response over the full responsive wavelength range, which is given by:

$$IR = \int |\Delta\%T(\lambda)| d\lambda \quad (S1)$$

where IR is the integrated response in units of (%T)nm and  $\Delta\%T(\lambda)$  is the change in percent transmission as a function of wavelength. This analytical protocol yields a single response curve that accounts for the broad responsive wavelength range of the crystals (middle panels of Figures S5(a) and S5(b)). These plots show the change in IR of the crystals as solutions of increasing concentration of PEG (increasing refractive index) are injected into the flow cell. The bottom panels of Figures S5(a) and S5(b) show that the IR is linearly related to the change in bulk refractive index of the PEG solution. The slope of the lines yield the multispectral bulk refractive index sensitivity of the crystals, which are ~41,000 and 13,000 (%T)nm/RIU for the 35 and 95nm thick gold crystals respectively. As suggested by the units, this metric weights both the shifts in the positions and intensities of the resonances across the spectrum as the bulk refractive index of the solution is changed. Since this multispectral analysis method is new, these integrated bulk refractive index sensitivities cannot be directly compared to the bulk refractive index sensitivity values reported in the literature for LSPR and SPR sensors.[4]

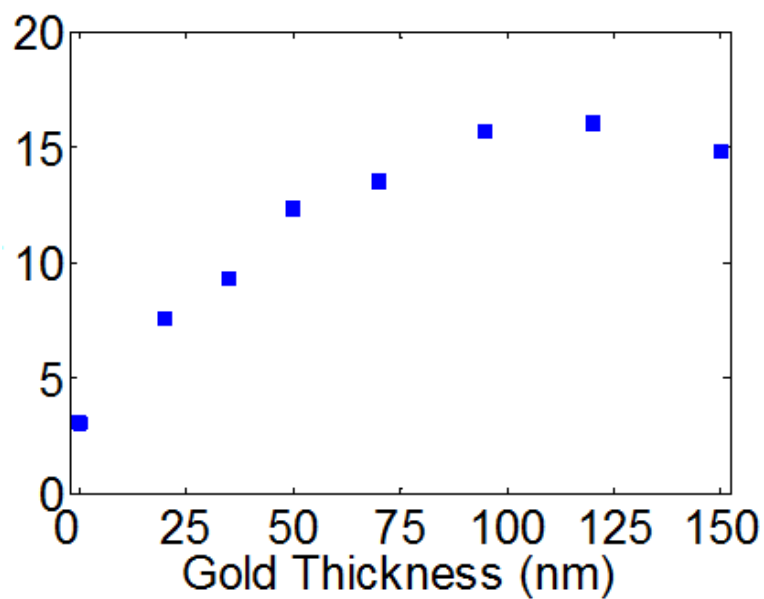


**Figure S6.** The sensitivity of crystals (~728 nm periodicity) to thin polyelectrolyte films as a function of the gold thickness on the plasmonic crystal. The sensitivity is reported as the change in integrated response per nanometer of polyelectrolyte ( $\Delta\text{Int. Resp./nm}$ ). These results agree well with the results obtained from electrodynamics modeling of the crystals and from bulk refractive index sensitivity measurements.

References:

- [1] Stewart, M. E.; Mack, N. H.; Malyarchuk, V.; Soares, J. A. N. T.; Lee, T.-W.; Gray, S. K.; Nuzzo, R. G.; Rogers, J. A. *Proc. Natl. Acad. Sci. U.S.A.* **2006**, *103*, 17143-17148.
- [2] Jung, L.S.; Campbell, C.T.; Chinowsky, T.M.; Mar, M.N.; Yee, S.S. *Langmuir* **1998**, *14*, 5636–5648.
- [3] Yao, J.; Stewart, M. E.; Maria, J.; Lee, T.-W.; Gray, S. K.; Rogers, J. A.; Nuzzo, R. G. *Angew. Chem., Int. Ed.* **2008**, *47*, 5013-5017.
- [4] Shumaker-Parry, J. S.; Campbell, C. T. *Anal. Chem.* **2004**, *76*, 907-917.